# Implementation of Double Loop Controller Tuned Super Lift Luo Converter and Unipolar Inverter for Solar Fed Grid Application

P.Nammalvar *‡, S.Ramkumar **, P.Meganathan ***, S.Ramesh****

*Department of Electrical and Electronics Engineering, Krishnasamy College of Engineering and Technology, Cuddalore, Tamilnadu, India – 607109

**Department of Electrical and Electronics Engineering, United Institute of Technology, Coimbatore, Tamilnadu, India – 641020

***Department of Electrical and Electronics Engineering, Sri Venkateshwaraa College of Engineering and Technology, Ariyur, Puducherry India – 605102

****Department of Computer Science and Engineering, Krishnasamy College of Engineering and Technology, Cuddalore, Tamilnadu, India – 607109

(alvar1976@gmail.com, ramme04@gmail.com, megaisagem@gmail.com, swami.itraj@gmail.com)

‡ Corresponding Author: Dr. P. Nammalvar, Associate Professor/EEE, Krishnasamy College of Engineering and Technology, Cuddalore, Tamilnadu, India-607109, Tel: +91 9976228603, alvar1976@gmail.com

*Received: 28.12.2020 Accepted:15.01.2021*

**Abstract-** The main objective of this article is to generate Photovoltaic (PV) power generation with high power quality before it is connected to the grid. The PV side DC/DC conversion is done by Positive Output Elementary Super Lift Luo converter (POESLLC) with high voltage conversion ratio for better performance. The grid side AC conversion is achieved by adding a double loop controller and it is used to ensure less voltage variation in grid voltage during for line and load variations. DC power received from the solar panel is stabilized in the POESLLC converter with double loop controller, which consists of a PI controller on the outer loop and hysteresis current controller inner loop. In the second stage, open-loop Pulse Width Modulation (PWM) based unipolar full-bridge inverter is used to meet the power quality issues. This modified system avoids the closed-loop controller for inverter on grid side and also omits the Maximum Power Point Tracking (MPPT) algorithm in DC/DC conversion. The proposed system has some advantages such as fewer components, less weight and avoids complexity in controllers which inject steady current to the utility grid. The effectiveness of the converters is verified through MATLAB Simulink platform.

**Keywords** Solar PV; Double loop controller; Hysteresis current controller; Single Phase Unipolar Inverter (SPUPI); Luo Converter.

## 1. Introduction

The electricity supplied by a PV power generation unit depends on the solar insolation and temperature. In tropical countries, the availability of solar power in abundance, hence the photovoltaic system can meet the emerging power demand. The initial expenditure, however, decreases the importance of the solar PV system even if there are virtually no operating costs and repair costs. PV panel cost alone approximately 57 % of the system total cost, the battery cost [1] is around 30 % and the inverter cost along with MPPT control is around 7 % [2]. Numerous researches are going in the PV technology to reduce cost efforts. The cost of PV is anticipated to drop significantly per watt by 2020. On the other hand, the cost of other components [3] (DC/DC converter and inverter components, storage devices, instrumentation, etc.) must be reduced to reduce the total cost of a PV system. At PV cell level, the instrumentation involved in MPPT can be minimized [4]. In this article, to increase efficiency without MPPT and minimize cost

expenditure, a double loop controller is introduced. The purpose of this research article is to harvest high-quality electricity from solar PV to minimize dependence on fossil fuels and to reduce energy usage costs by allowing grid connections [5]. Removal of storage batteries and complicated MPPT which is the most expensive system components per watt can be done using this system.

The expense is further lowered for on-grid PV systems due to the absence of the battery bank, which seems to be the second major source to the cost of the PV system. By reducing the number of power conversion stages [6] and the number of components involved in each phase, the performance of the on-grid network can also be improved. Since transformers have inherent protection against DC injection into the grid [7], the inverters without the transformer require extra electronics to minimise DC injection to the lowest permissible level (Allowable DC injection limit different from country to country based on their regulations). However, the non-transformer configuration is electrically more efficient, with the transformer accounted for about 2% of peak efficiency. The circuit is framed in this configuration without a bulky transformer.

Normally DC/DC converters have been used widely as front end converter for solar power applications. The POESLLC represents the start of DC/DC converter [8] and positive source-side voltage is also transferred to the load side positive voltage. This converter maintains high voltage gain, high density of power, improved efficiency, lower ripple current and voltage. These converters are more commonly applied in industrial applications, electronic devices and switched mode power supply, especially in low voltage projects to high voltage [9] and [10].

In this paper, the first stage DC/DC conversion was done by POESLLC. The proposed POESLLC operates with a double loop controller which consists of a PI controller in outer loop and hysteresis current controller in inner loop. By comparing the traditional single-loop PI controller with POESLLC, the performance of the proposed system is analysed. Besides, the gird integrated PWM-based Voltage Source Inverter (VSI) [11] commonly used in PV systems, performing two functions at least, due to the unique features of PV modules. First, the inverter's DC input voltage should be balanced to a specific value because the PV modules output voltage varies with temperature, irradiance, and MPPT effect [12]. Secondly, the power from PV modules should be fed into the utility grid by transforming the DC current into a synchronized sinusoidal waveform with the utility grid.

An AC output is obtained from a DC input in the inverter circuit by an effective switching scheme sequence. The PWM technology is employed in this model to control switching operation. The process of switching is unipolar. The VSI is one with small or insignificant impedance in the DC source. This unipolar inverter aims to produce a fixed frequency and high-performance operation. For the four switch inverter, PWM is used to adjust the switching frequency and produce the correct switching. The grid-connected inverter [13] would control the current against both the grid voltage and the line impedance. It was found that the operation of the grid-connected inverter to be quite dependent on the operating conditions. Utility-interactive systems are more critical for reducing the harmonic components in the output current to a limited amount. Under varying atmospheric conditions, the MPPT's purpose is to change the solar voltage to the Maximum Power Point (MPP). In this article, a simple approach combining a discrete-time control and a PI compensator is used to track the MPPs of solar arrays. If the PV system functions at the MPP of the PV, the controller will continue to test. To control the system it should leverage continuously by measuring voltage and current and [14] forcing the system to track this MPP. The command parameter of the variable to be controlled is the power supplied to the load. The *dp/dv* is forced to zero to harvest possible power from PV arrays. This control mechanism does not alter the PV array characteristics but maximizes the load capacity and not the output power of the PV array [15]. Partial shadows allowed the trackers lose control of the MPP in a short period, so the MPP rapidly shifted away and then moved back to the original position, which was equal to the energy lost when the array would be shifted the MPP. If the solar insolation changes, the tracker must react within a short time to avoid loss of energy. The controller should, therefore, be able to adjust and manage the PV always at its MPP.

## 2. Simplified Model of PV Panel

When exposed to sunlight, the PV system can generate DC without any environmental impact. The basic functional part of PV arrays was its solar cell [16], which is essentially an optoelectronic device with a P-N junction which transforms light directly into electrical energy. The PV module output depends on the cell temperature, the solar insolation and the PV output voltage. Fig.1 displays the equivalent circuit of the solar PV cells.

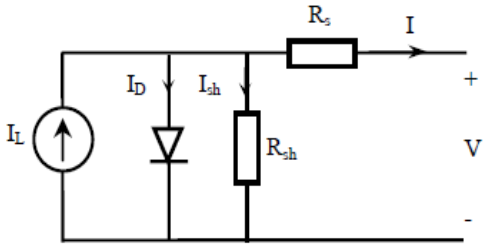


**Fig. 1.** Solar PV cell equivalent circuit.

The most important fundamental equation defining the characteristics of the PV model (*I-V*) [17] is shown in equation (1).

$$I = I_L - I_o(e^{\frac{q(v+IR_S)}{KT}} - 1) - \frac{V + IR_S}{R_{sh}} \quad (1)$$

$I$ - Cell current (A).

$I_L$ - Light generated current (A).

$I_o$ - Diode saturation current.

$q$ - Charge of electron = 1.6 X 10¯19 (coul).

$K$ - Boltzman constant (j/K).

$T$ - Cell temperature (K).

$R_s$, $R_{sh}$ - Series and shunt resistance (ohms).

$V$ - Cell output voltage (V)

The output of a PV cell can only be determined if there is knowledge of the open-circuit voltage, short-circuit current and voltage at the MPP. Obtaining MPP is very simple. The first step is to plot the PV cell's voltage $V_s$ power graph. By multiplying the voltage and the corresponding current through the cell, power is measured. The MPP shall be measured from the plot and the resulting voltage shall be observed. The next step is to locate the current corresponding to the voltage at MPP according to the cell's *V-I* characteristics. This current refers to $I_{mp}$ is called the current at MPP. The meeting point at which $I_{mp}$ and $V_{mp}$ are the MPP and it is shown in Fig. 2. The operating point is the point at which maximum power is available in the PV cell. If this stage is precisely reached by the load line, the full power would be transferred to the load.

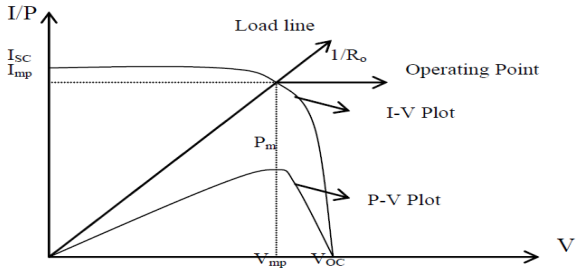


**Fig. 2.** PV output characteristics of solar array

## 3. Proposed System

In this paper, the double loop controller is designed and implemented for solar PV fed grid system to keep less variation and to maintain the grid voltage constant for line and load variations. In this controller, the PI current controller for the outer loop and inner loop hysteresis is taken into account. The proposed system block diagram is shown in Fig. 3.

This topology consists of PV panel, POESLLC, SPUPI and output filter. In this block, the grid voltage is controlled by control logic consists of PI controller and hysteresis loop current controller. The PWM based unipolar switching drives the IGBT present in the inverter is to convert DC into AC and to maintain the quality of the system before it was connected to the utility grid.

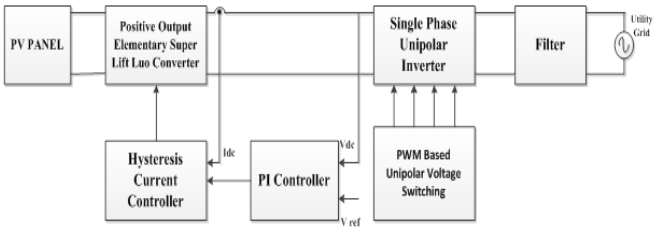


**Fig. 3.** Proposed System Block diagram

The layout of the connected PV system with a single phase grid is shown in Fig. 4. The system is composed of PV panel, POESLLC, Single Phase Unipolar Inverter and Output filter with grid. The effective design of POESLLC produces steady state DC voltage. The solar panel output is not continual constant and is proportional to the intensity of sunlight and ambient temperature.

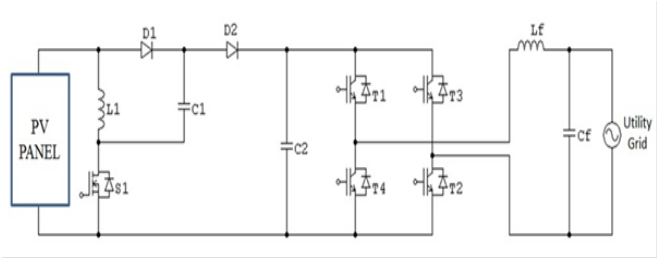


**Fig. 4.** Circuit Diagram of proposed system

The DC output from POESLLC is converted into AC by SPUPI and then fed into the central utility grid after which it is distributed to customers. In this circuit, the inductance ($L_f$) and the output capacitor ($C_f$) acting as an output filter [18], it aids to smooth the PWM inverter before the voltage reaches the utility grid.

## 4. Modeling of Positive Output Elementary Super Lift Luo Converter

During the switch-on and switch-off, the fundamental and its equivalent circuits were shown in Figs.5. For its excellent fast switching characteristics [19], extremely high *dv/dt* capability, and high current and voltage levels, the converter switch (MOSFET) is selected. In addition to these important features [20], the cost of this MOSFET is relatively modest. At the transfer site where it was connected to the MOSFET, a suitable heat sink is used to enhance the dissipation of heat generated through rapid switching and flowing currents. The input of converter is $V_{in}$ and consists of several passive components like inductor $L_1$ and capacitors $C_1$ & $C_2$, the active power switch (n-channel MOSFET) $S_1$, the freewheel diodes $D_1$ and $D_2$ and the load resistance $R_L$.

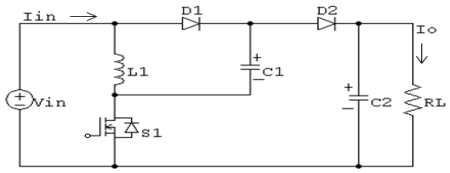


**Fig. 5 (a).** Elementary Circuit

Mode 1: Once the $S_1$ switch is activated, the voltage is charged to $V_{in}$ via capacitor $C_1$. The current $i_{L1}$ flows through the $L_1$ inductor raises with the $V_{in}$ voltage.

Mode 2: When the $S_1$ switch is turned off, the voltage decreases ($V_o$-2 $V_{in}$). Thereupon, the $i_{L1}$ ripple of inductor current is given as equation (2),

$$\Delta_{iL1} = \frac{V_{in}}{L_1} dT = \frac{V_o - 2V_{in}}{L_1}(1-d)T \tag{2}$$

The output voltage of the converter is given by equation (3)

$$Vo = \frac{2-d}{1-d} Vin \tag{3}$$

The voltage transfer gain equation mentioned in (4)

$$G = \frac{V_o}{V_{in}} = \frac{2-d}{1-d} \tag{4}$$

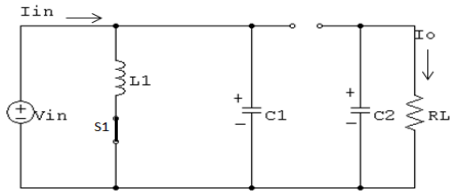


**Fig. 5 (b).** Elementary Circuit when switch turn ON

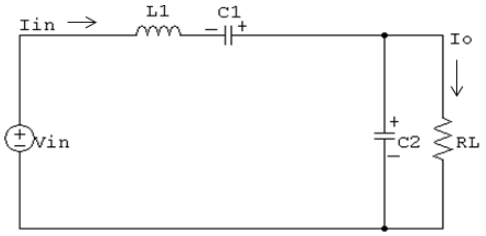


**Fig. 5 (c).** Elementary Circuit when switch turn OFF

During switch-on, the in input current is equal to ($i_{L1}$ + $i_{C1}$) and during switch-off only equal to $i_{L1}$. The average charge on the $C_1$ capacitor does not change in a steady state. We have the related equation (5) following:

$$\begin{aligned} i_{in-off} &= i_{L1-off} = i_{c1-off} \\ i_{in-on} &= i_{L1-on} + i_{c1-on} \\ dTi_{c1-on} &= (1-d)Ti_{c1-off} \end{aligned} \tag{5}$$

If the $L_1$ inductance is high enough, the $i_{L1}$ is almost equal to the average current of $I_{L1}$.

Therefore related equation (6) gives

$$\begin{aligned} i_{in-off} &= i_{c1-off} = I_{L1} \\ i_{in-on} &= I_{L1} + \frac{1-d}{d} I_{L1} = \frac{I_{L1}}{d} \\ i_{C1-on} &= \frac{1-d}{d} I_{L1} \end{aligned} \tag{6}$$

and the average input current shown in (7)

$$I_{in} = di_{in-on} + (1-d)i_{in-off} = I_{L1} + (1-d)I_{L1} = (2-k)I_{L1} \tag{7}$$

In consideration input power given by equation (8)

$$\frac{Vin}{Iin} = \left(\frac{(1-d)}{(2-d)}\right)^2 \frac{Vo}{Io} = \left(\frac{(1-d)}{(2-d)}\right)^2 R \tag{8}$$

The ratio of $i_{L1}$ current to $L_1$ inductor variance has arrived in equation (9)

$$\xi_1 = \frac{\Delta i_{L1}/2}{I_{L1}} = \frac{d(2-d)TV_{in}}{2L_1 I_{in}} = \frac{\mathrm{d}(1-d)^2}{2(2-d)fL_1} \tag{9}$$

The above equation suggests that this converter typically operates in continuous mode, generally small (much smaller than unity). The output voltage ripple $V_o$ is given by (10)

$$\xi = \frac{\Delta v_o/2}{V_o} = \frac{1-d}{2RfC_2} \tag{10}$$

The state variables $V_1$, $V_2$ and $V_3$ are selected as $i_{L1}$ current, $V_{C1}$ voltage and $V_{C2}$ voltage, respectively.

Whenever the circuit is closed, the equation of POESLLC state space is given as in (11)

$$\begin{cases} V_1 = \dfrac{v_{in}}{L_1} \\ V_2 = \dfrac{V_{in}}{C_1 R_{in}} - \dfrac{V_1}{C_1} \\ V_3 = -\dfrac{V_3}{RC_2} \end{cases} \tag{11}$$

Whenever the circuit is opened, the equation of POESLLC state space is given as in equation (12)

$$\begin{cases} V_1 = \dfrac{v_{in}}{L_1} - \dfrac{v_2}{L_1} - \dfrac{v_3}{L_1} \\ V_2 = \dfrac{V_1}{C_1} \\ V_3 = -\dfrac{V_1}{C_2} - \dfrac{v_3}{RC_2} \end{cases} \tag{12}$$

By using the method of state space averaging, the POESLLC state space averaging model is given as in (13) and (14).

$$\begin{bmatrix} \dfrac{di_{L2}}{dt} \\ \dfrac{dV_{C1}}{dt} \\ \dfrac{d_{VC2}}{dt} \end{bmatrix} = \begin{bmatrix} \dfrac{1}{R_{in}L_1} & \dfrac{d-1}{L1} & \dfrac{d-1}{L1} \\ \dfrac{1-2d}{C_1} & \dfrac{-d}{RinC_1} & 0 \\ \dfrac{1-d}{C_2} & 0 & -\dfrac{1}{RC_2} \end{bmatrix} \begin{bmatrix} V_1 \\ V_2 \\ V_3 \end{bmatrix} + \begin{bmatrix} \dfrac{1}{L_1} \\ \dfrac{d}{R_{in}C_1} \\ -\dfrac{i_{L1}}{C_2} \end{bmatrix} u \tag{13}$$

$$\boldsymbol{v} = A\boldsymbol{v} + B\boldsymbol{u} \tag{14}$$

Its output equation is given as in (15)

$$V_o = v_4 \tag{15}$$

If $R_{in}$ is the internal source resistance that is not used in the circuit but it is a negligible value, $u$ is input vector, $d$ is the duty cycle, the vectors of the state variables ($i_{L1}$, $V_{C1}$, $V_{C2}$) and their derivatives. Where $R_{in}$ is a source's internal resistance that is not shown in the circuit but is a very small value, $u$ is an input variable. Next, $d$ is duty cycle, vectors of the state variables ($i_{L1}$, $V_{C1}$, $V_{C2}$) and their derivatives respectively.

## 5. Modeling of Unipolar Single Phase Inverter

The first task is to choose the switches that are used in the inverter. IGBT switches are used which is the combination of a MOSFET and a BJT. The advantages of both switches are a good trade-off. As well as relatively high switching speed capabilities, they have high power capacity, low on-state resistance [21]. Their high voltage capabilities make them appropriate for our application. The basic principle of generating pulse for unipolar inverter is shown in Fig. 6. In contrast to bipolar voltage switching, the unipolar voltage switching scheme has a superior harmonic profile. For this purpose, unipolar voltage switching for the single phase inverter is used as a switching scheme.

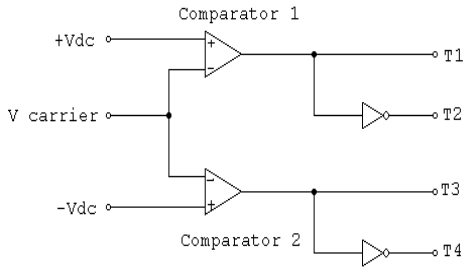


**Fig. 6** Unipolar PWM generator

The two familiar types of PWM techniques suitable for single phase inverters are bipolar and unipolar techniques. To afford positive outputs unipolar PWM exert $+V_{DC}$ and zero. Next, to afford negative outputs PWM exerts $-V_{DC}$ and zero, but the bipolar PWM uses the only $+V_{DC}$ and $-V_{DC}$ to get negative or positive outputs. Consequently, the bipolar scheme of carrier harmonic content is twice of unipolar scheme. Also, the output of the unipolar scheme contains very minimal even harmonics. But the high-frequency harmonics present around twice of switching frequency. Because of these desirable features of the unipolar PWM, it's developed in this paper. DC output from the POESLLC is the input to the inverter stage and the output is connected to the grid, as seen in Fig. 7 and Figs.8.

The equation for inverter AC output voltage is mentioned in (16)

$$V_{out} = V_{DC} \times m \times \sin(2\pi f_o t) \tag{16}$$

The notations $V_{out}$, $V_{DC}$, $m$, and $f_o$ is taken as the inverter AC output voltage, Inverter DC input voltage, PWM modulation index, and Inverter output voltage frequency, respectively. The state equations can be written as assuming ideal elements as mentioned in below equation (17).

$$\begin{cases} L\dfrac{di_L}{dt} = u \times V_{DC} - V_{out}; Where - u = -1, 0, +1 \\ C\dfrac{dV_{out}}{dt} = i_c = i_L - i_o \\ i_o = \dfrac{V_{out}}{R} \end{cases} \tag{17}$$

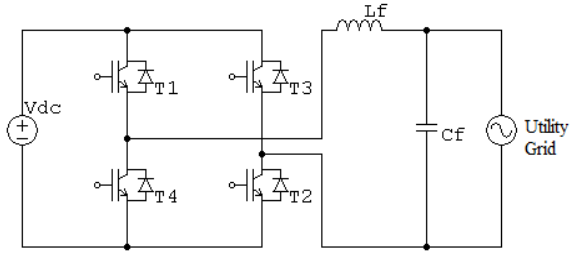


**Fig. 7** PWM base single phase inverter

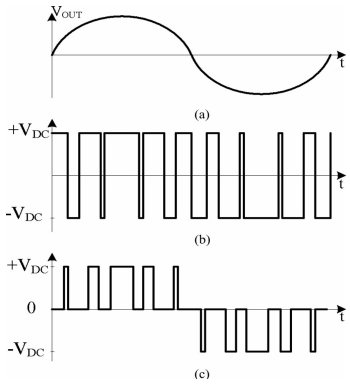


**Fig. 8** (a). Sinusoidal output voltage of inverter. (b) PWM pattern of Bipolar (c) PWM pattern of Unipolar

The state variables considered here are inductor current $i_L$ and the inverter output voltage $V_{out}$. The discontinuous input of the system is notated by '$u$'. To afford positive output PWM sends 0 or 1 and, 0 or −1 to afford negative output. Further, the current through the capacitor, inverter output current and load resistance are notated by $i_c$, $i_o$, and $R$ respectively.

To synchronize the system with the grid, there are three conditions. First, the system's output should have the same frequency as the main one (50Hz). Then, it must be in phase and before attempting synchronization, the output voltage should have the same amplitude. Lastly, it must match with the voltage amplitude of the grid. The first two conditions are satisfied by the sine wave that compared to the triangular wave generated through a step-down transformer which is used for circuit operating voltage that senses the grid. The last condition is to check the voltage amplitude of the grid and it is ensured by the double loop controller of the system.

## 6. Controller Design Aspects

### *6.1. Design of PI controller*

Ideal integral compensation is also known as PI Control. Difference between the reference input and actual input

produces an error component. To get the desired output, the values of $K_p$ and $K_i$ must be chosen accordingly. For DC/DC converter applications, controllers operating on the PI method are widely used. The ratio of output response to errors is calculated by the proportional gain of $K_p$. To overcome the steady state errors, the integral part integrates the error over time. Therefore, the integral response continuously increases with overtime unless the error is zero.

The PI output equation in discrete form can be written as in (18)

$$Y(n) = Kp\ e(n) + Ki \sum n\ k= 0\ \ e(k) \tag{18}$$

The proportional and integral components can be shown as separate transfer functions in parallel.

A typical PI compensator controller block G shown in Fig. 9. Taking the PI transfer function *G(s)* into account, the voltage error *E(s)* and the closed loop transfer function *T(s)* are given below. The equivalent transfer function of the compensator is also given. The location of the zero can be adjusted by adjusting $K_i / K_p$ as mentioned in equations (19), (20) and (21)

$$G(s) = k_p + \frac{k_i}{s} \tag{19}$$

$$E(s) = (V_{ref}(s) - V_{C_2}(s)) \tag{20}$$

$$\mathrm{T(s)} = \frac{V_{pv}(s)}{V_{ref}(s)} = \frac{k_p s + k_i}{C_2 s^2 + k_p s + k_i} \tag{21}$$

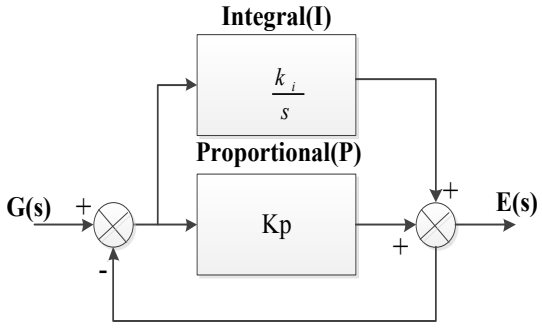


**Fig. 9** PI Controller Block

The *T(s)* transfer function is designed to account for a classic relationship between the closed-loop voltage settling time $t_S$ and the *Tsw* minimum switching period

The *T(s)* structure gives the following relations (22) and (23):

$$k_p = 2C_2 \zeta \omega_n \tag{22}$$

$$k_i = C_2 \omega^2{}_n \tag{23}$$

So the corresponding time constant description is used by the equivalent time constant definition, it is mentioned in (24)

$$\tau = 1 / \zeta \omega_n \tag{24}$$

It should be noted that all the desired outputs are achieved by the built PI controller. Nevertheless, a simpler proportional controller could be used at the steady-state error, the error is compensated for by the operation of the DC to DC converter.

Where $K_p$ and $K_i$ are PI controller settings. This controller's tuning is achieved using the form of the reaction curve. The PI control settings $K_p$ and $K_i$ are designed using the Ziegler-Nichols tuning technique based on the open loop response of the converter. Controller tuning requires choosing $K_p$ and $K_i$ best values. This is often an individual-based subjective process. The values of $K_p$ and $K_i$ are taken as $K_p$ = 0.003, $K_i$ = 0.4 in this work. It is noted that the configuration PI controller regulates the output voltage with a fast settling time. The over-shooting and settling time is less compared to the open loop in the closed loop PI controller, and also less oscillatory.

### *6.2. Design of hysteresis current controller*

As the fastest and easiest control procedure, hysteretic current control is considered. This paper provides the DC/DC POESLLC converter using the current control system for hysteresis. The new control approach of hysteresis has a quick and robust solution with basic architecture and easy implementation. If load transient happens, the hysteresis controllers respond fast. For feedback loop compensation, they do not require additional components. The elimination of the compensation network makes it easier to respond quickly to transient responses. This reduces the volume of theoretical part analysis and execution size and hence reduces the commitment to design.

There are two main limitations of the hysteresis-controlled converter: variable switching frequency and non-zero steady-state errors. By placing series connected PI block with voltage feedback, the non-zero steady-state error can be resolved. Through adjusting both the peak inductor current and the valley inductor current, the hysteretic current-mode control is controlled. The operation did not require an external oscillator or a saw-tooth generator and is capable of delivering rapid response under transient conditions. A block diagram of the hysteretic-controlled current-mode DC/DC converter can be seen in Fig.10.

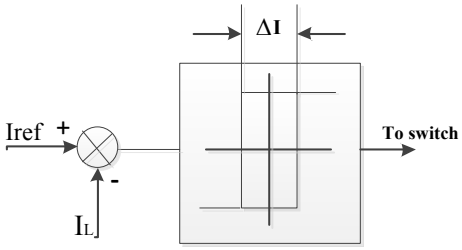


**Fig. 10** Hysteresis Current Control

Generally, the feedback-controlled power converter circuit is composed of power switch, inductor, capacitor and diode. Internal controller maintaining the working principle

of the converter by switching the topology of the circuit. The external controller adjusts the internal loop relation in response to variations of the desired output. The control mechanism as seen in Fig. 11, consisting of dual control loops. One is the current control loop and the other is the voltage control loop. The error between the actual output voltage and the reference voltage resulted an error value. For the regulation of hysteresis, a P or PI control block can use a voltage error signal to provide a reference current. The present hysteretic control system can also be interpreted as a sliding mode control scheme.

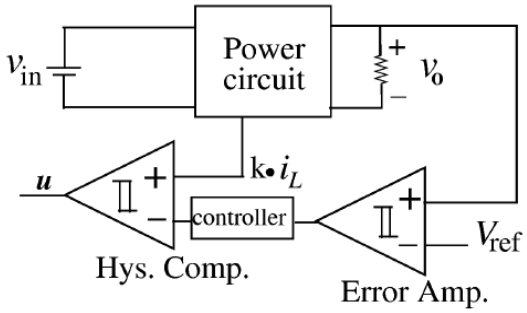


**Fig. 11** Double loop Controller Block

The hysteretic comparator applies the law of control using (25)

$$u = \begin{cases} 1, & S > 0 \\ 0, & S < 0 \end{cases} \tag{25}$$

The sliding surface (S) is measured by difference between the inputs of the comparator by the equation (26).

$$S = K_p(v_{ref} - vo) - k.i_L \tag{26}$$

Where k is the current sensing gain that has a fixed value and $K_p$ is the proportional gain considered here as the proportional controller. Two sets of differential equations will describe the POESLLC power circuit, which is mentioned in (27).

$$L\frac{di_L}{dt} = v_{in} - v_o \quad \text{and} \quad C\frac{dv_c}{dt} = i_L - \frac{v_o}{R} \tag{27}$$

The control system's two state variables are $x_1 = v_{ref} - v_0$ and $x_2 = i_L$ then the derivatives are given by equations (28) - (31).

$$L\dot{x}_2 = v_{in} - v_{ref} + x_1 \tag{28}$$

$$\Rightarrow \dot{x}_2 = \frac{1}{L}x_1 + \frac{v_{in}}{L} - \frac{v_{ref}}{L} \tag{29}$$

$$x_2 = C\dot{x}_1 + \frac{v_{ref} - x_1}{R} \tag{30}$$

$$\Rightarrow \dot{x}_1 = -\frac{x_2}{C} - \frac{x_1}{RC} + \frac{v_{ref}}{RC} \tag{31}$$

In terms of state variables, the state space model is given by (32) and (33),

$$\dot{x} = A_1 x + B_1 u + D; \tag{32}$$

$$\begin{bmatrix} \dot{x}_1 \\ \dot{x}_2 \end{bmatrix} = \begin{bmatrix} -\frac{1}{RC} & \frac{1}{C} \\ -\frac{1}{L} & 0 \end{bmatrix} \begin{bmatrix} x_1 \\ x_2 \end{bmatrix} + \begin{bmatrix} 0 \\ \frac{v_{in}}{L} \end{bmatrix} u + \begin{bmatrix} 0 \\ \frac{v_{ref}}{L} \end{bmatrix} \tag{33}$$

where '*u*' is a discontinuous input. The value of '*u*' is either 0 or 1.

## 7. Simulation Results

The simulations have been performed on the POESLLC circuit and single phase unipolar inverter with parameters specified in Table 1. The dynamic and static performances of these converters are evaluated with conventional PI control and double loop controller using MATLAB/SIMULINK.

**Table 1** Simulation Parameters

| Description | Parameter | Typical Value |
|---|---|---|
| PV Panel Voltage | *Vin* | 90 V |
| Grid Voltage | *Vgrid* | 230 V |
| PV Panel Current | $I_{in}$ | 2.44 A |
| Maximum PV Power | $M_{PPP}$ | 220 W |
| Inductor | $L_1$ | 0.5 mH |
| Capacitor | $C_1, C_2$ | 1000 µF |
| Switching Frequency of POESLLC | $f_s$ | 20 KHz |
| Duty cycle range of POESLLC | *d* | 0.4 to 0.6 |
| Desired duty cycle of POESLLC | *d* | 0.5 A |
| Grid Current | $I_{grid}$ | 0.9 A |
| Grid Voltage and Current THD | $V_{THD}$ & $I_{THD}$ | < 5 % |
| Output Power | $P_{out}$ | 220 W |
| Grid Frequency | $f_g$ | 50 Hz |
| Efficiency | µ | >97 % |

### *7.1. Simulation Analysis of POESLLC*

#### *7.1.1. Transient Condition*

The DC voltage output of the POESLLC with PI control and double loop control in a transient condition. It could be observed that at the time of 0.03 sec the voltage output of the converter was settled in the developed PI control but in case of double loop controller, output has settled at the time of 0.02 sec which is much faster than the previous one shown in Fig.12.

The DC output current of POESLLC with PI control and double loop control at transient condition. It could be observed that it was at the time of 0.09 sec the output current of the converter was settled in the designed PI control but in case of double loop controller, output has settled at the time of 0.04 sec which is much faster than the previous one as shown in Fig.13. From Fig. 12 and Fig. 13, it is expected that the double loop controller can be preferably used in practice.

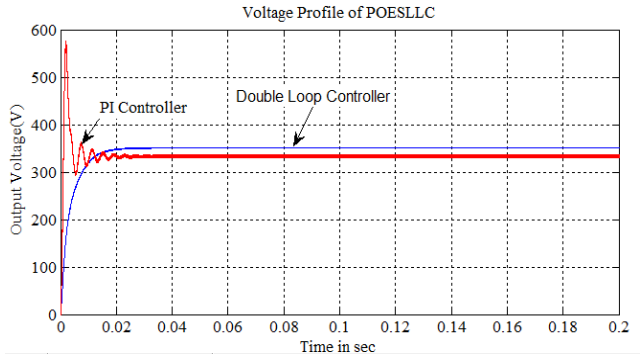


**Fig. 12** DC output Voltage of POESLLC using double loop controller and PI controller

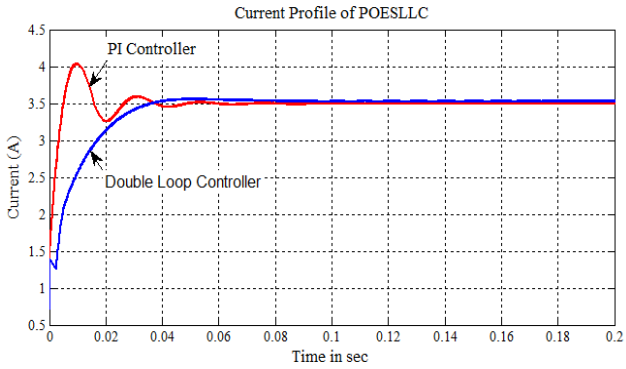


**Fig. 13** DC output current of POESLLC using double loop controller and PI controller

### *7.2. Simulation Analysis of SPUPI*

#### *7.2.1. Output Voltage of SPUPI (Grid voltage)*

Response of the output voltage of single phase unipolar inverter using PI controller and double loop controller is implemented in front end POESLLC as shown in Fig.14.

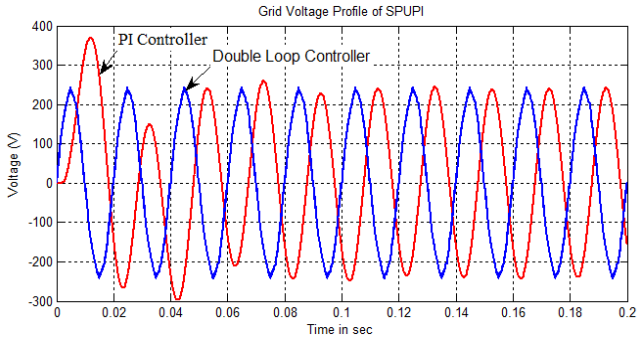


**Fig. 14** AC output voltage of SPUPI (Grid Voltage)

#### *7.2.2. Output Voltage of SPUPI (Grid current)*

The response of the output current at full load condition of single phase unipolar inverter using PI controller and double loop controller is implemented in front end POESLLC and it is displayed by Fig.15.

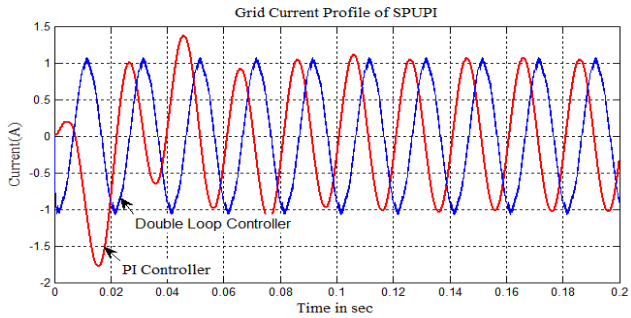


**Fig. 15** AC output voltage of SPUPI (Grid Current)

#### *7.2.3. Total Harmonic Distortion*

Harmonic distortion is the deviation from the ideal sinusoidal waveform in the waveform of the supply voltage or current. It creates significant adverse effects in grid power integration. Standards specify the major harmonic voltage or current occurring on the network, typical of which is 5% total harmonic distortion.

The total harmonic distortion of the voltage and current of the grid for both topologies as seen in Figs.16. The voltage and current THD of the proposed converter also meets the IEEE and IEC standards.

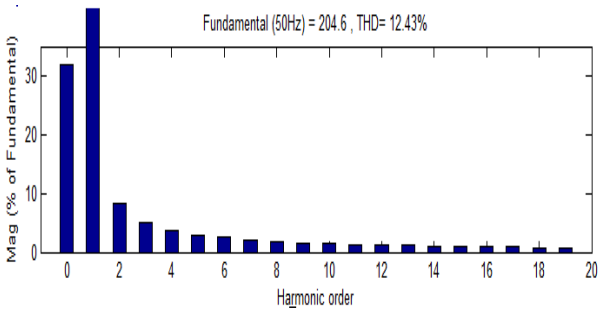


**Fig. 16(a)** Current THD of grid using PI controller

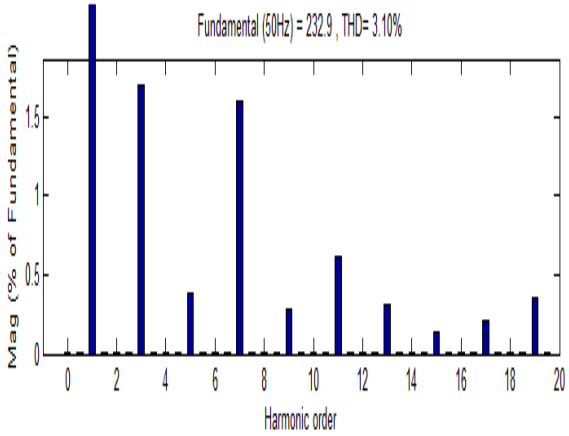


**Fig. 16(b)** Current THD of grid using double loop controller

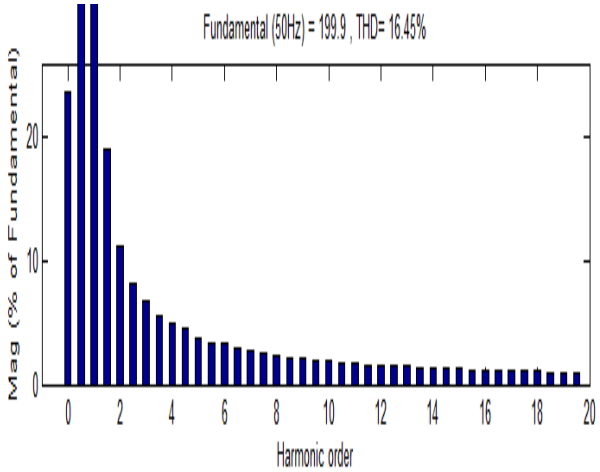


**Fig. 16(c)** Voltage THD of grid using PI controller

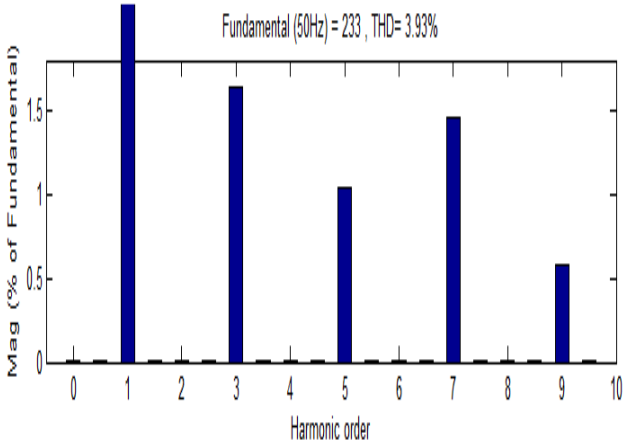


**Fig. 16(b)** Voltage THD of grid using double loop controller

## 8. Conclusion

For solar fed applications, a new combination of grid connected solar power conditioning systems with POESLLC and SPUPI has been developed and implemented. The conventional PI control and double loop control systems have proven the robustness of the conversion of DC/DC and DC/AC in this article. The significant feature of this system is that the inverter does not require references for to the controlling grid voltage or current and also avoids control of the MPPT. It is also very easy to incorporate without any difficulties and because of fewer components, it is cost-effective. The output of the proposed system is evaluated by simulation analysis. This would be expected that the proposed double loop controller method could be used preferably in practice. The key aim of this study is to improve green energy users.

## References

[1] G. Todeschini, H. Huang, N. Bristow, T. W. David, and J. Kettle, "A Novel Computational Model for Organic PV Cells and Modules," *Int. J. Smart Grid - ijSmartGrid*, vol. 4, no. 4, Art. no. 4, Dec. 2020.

[2] A. Nazer, S. Driss, A. M. Haddadi, and S. Farhangi, "Optimal Photovoltaic Multi-String Inverter Topology Selection Based on Reliability and Cost Analysis," *IEEE Trans. Sustain. Energy*, 2020.

[3] A. I. Nusaif and A. L. Mahmood, "MPPT Algorithms (PSO, FA, and MFA) for PV System Under Partial Shading Condition, Case Study: BTS in Algazalia, Baghdad," *Int. J. Smart Grid - ijSmartGrid*, vol. 4, no. 3, Art. no. 3, Sep. 2020.

[4] N. Kumar, I. Hussain, B. Singh, and B. K. Panigrahi, "Framework of maximum power extraction from solar PV panel using self predictive perturb and observe algorithm," *IEEE Trans. Sustain. Energy*, vol. 9, no. 2, pp. 895–903, 2017.

[5] F. Ayadi, I. Colak, I. Garip, and H. I. Bulbul, "Impacts of Renewable Energy Resources in Smart Grid," in *2020 8th International Conference on Smart Grid (icSmartGrid)*, Jun. 2020, pp. 183–188, doi: 10.1109/icSmartGrid49881.2020.9144695.

[6] C. Wang, M. Li, Z. Ouyang, and G. Wang, "Resonant Push–Pull Converter With Flyback Regulator for MHz High Step-Up Power Conversion," *IEEE Trans. Ind. Electron.*, vol. 68, no. 2, pp. 1178–1187, Feb. 2021, doi: 10.1109/TIE.2020.2969109.

[7] Y. Furukawa, H. Tomura, T. Suetsugu, and F. Kurokawa, "Variable Feedback Gain DC-DC Converer Tracing Output Voltage Fluctuation for Renewable Energy System," in *2019 8th International Conference on Renewable Energy Research and Applications (ICRERA)*, Nov. 2019, pp. 916–921, doi: 10.1109/ICRERA47325.2019.8996540.

[8] M. Mahdavi, M. Shahriari-kahkeshi, and N. R. Abjadi, "An Adaptive Estimator-Based Sliding Mode Control Scheme for Uncertain POESLL Converter," *IEEE Trans. Aerosp. Electron. Syst.*, vol. 55, no. 6, pp. 3551–3560, Dec. 2019, doi: 10.1109/TAES.2019.2908272.

[9] X. Yuan, I. Laird, and S. Walder, "Opportunities, Challenges, and Potential Solutions in the Application of Fast-Switching SiC Power Devices and Converters," *IEEE Trans. Power Electron.*, vol. 36, no. 4, pp. 3925–3945, Apr. 2021, doi: 10.1109/TPEL.2020.3024862.

[10] H. Wang, A. Gaillard, and D. Hissel, "A review of DC/DC converter-based electrochemical impedance spectroscopy for fuel cell electric vehicles," *Renew.*

*Energy*, vol. 141, pp. 124–138, Oct. 2019, doi: 10.1016/j.renene.2019.03.130.

[11] A. R. A. Manito, A. Pinto, and R. Zilles, "Evaluation of utility transformers' lifespan with different levels of grid-connected photovoltaic systems penetration," *Renew. Energy*, vol. 96, pp. 700–714, Oct. 2016, doi: 10.1016/j.renene.2016.05.031.

[12] E. Kurt and G. Soykan, "Performance Analysis of DC Grid Connected PV System Under Irradiation and Temperature Variations," in *2019 8th International Conference on Renewable Energy Research and Applications (ICRERA)*, Nov. 2019, pp. 702–707, doi: 10.1109/ICRERA47325.2019.8996577.

[13] H. Mirshekali, R. Dashti, H. R. Shaker, and R. Samsami, "A New Model Predictive Control Based Method for Control of Grid Connected Inverter Using Predictive Functional Control," in *2020 IEEE 8th International Conference on Smart Energy Grid Engineering (SEGE)*, Aug. 2020, pp. 22–26, doi: 10.1109/SEGE49949.2020.9181896.

[14] P. Nammalvar, R. Subburam, U. Ramkumar, and P. Kasinathan, "Crowded plant height optimisation algorithm tuned maximum power point tracking for grid integrated solar power conditioning system," *IET Renew. Power Gener.*, vol. 13, no. 12, pp. 2137–2147, 2019, doi: 10.1049/iet-rpg.2018.5053.

[15] P. Nammalvar, "Parameter Improved Particle Swarm Optimization Based Direct-Current Vector Control Strategy for Solar PV System," *Adv. Electr. Comput. Eng.*, vol. 18, no. 1, Art. no. 1, Feb. 2018, doi: 10.4316/AECE.2018.01013.

[16] N. Pachaivannan, R. Subburam, M. Padmanaban, and A. Subramanian, "Certain investigations of ANFIS assisted CPHO algorithm tuned MPPT controller for PV arrays under partial shading conditions," *J. Ambient Intell. Humaniz. Comput.*, Jan. 2021, doi: 10.1007/s12652-020-02738-w.

[17] K. Kajiwara, T. Kazuki, S. Ikeda, N. Matsui, and F. Kurokawa, "Performance Mechanism of Active Clamp Resonant SEPIC Converter in Renewable Energy Systems," in *2019 8th International Conference on Renewable Energy Research and Applications (ICRERA)*, Nov. 2019, pp. 1042–1046, doi: 10.1109/ICRERA47325.2019.8997086.

[18] D. Zhou, H. Wang, and F. Blaabjerg, "Reactive Power Impacts on LCL Filter Capacitor Lifetime in Grid-Connected Inverter," *IEEE Open J. Power Electron.*, vol. 1, pp. 139–148, 2020, doi: 10.1109/OJPEL.2020.2992279.

[19] W. Jiang, S. H. Chincholkar, and C. Chan, "Improved output feedback controller design for the super-lift re-lift Luo converter," *IET Power Electron.*, vol. 10, no. 10, pp. 1147–1155, 2017, doi: 10.1049/iet-pel.2016.0395.

[20] M. Tsai, C. Chu, and W. Chen, "Implementation of a Serial AC/DC Converter With Modular Control Technology," in *2018 7th International Conference on Renewable Energy Research and Applications (ICRERA)*, Oct. 2018, pp. 245–250, doi: 10.1109/ICRERA.2018.8566914.

[21] M. Pokharel, N. Hildebrandt, C. N. M. Ho, and Y. He, "A Fast-Dynamic Unipolar Switching Control Scheme for Single-Phase Inverters in DC Microgrids," *IEEE Trans. Power Electron.*, vol. 34, no. 1, pp. 916–927, Jan. 2019, doi: 10.1109/TPEL.2018.2818128.